Physica B 647 (2022) 414351

Contents lists available at ScienceDirect

Physica B: Physics of Condensed Matter

journal homepage: www.elsevier.com/locate/physb

Temperature sensing characteristics and first-principles simulation of Gd-doped $NaY(WO_4)_2$ phosphors

Hongbin Li [a,1], Jiaqi Zhao [b,1], Wenjing Yang [a], Tianqing Zhang [a], Mengjia Chen [a], Weiling Yang [a], Hongyuan Sha [d], Chun Li [a,c,*], Huisheng Liu [a,e], Yongtao Li [e], Zhiming Shi [f], Shanli Zhang [f], Hai Lin [a,c,**], Fanming Zeng [a,c,***], Zhongmin Su [a,c]

[a] School of Materials Science and Engineering, Changchun University of Science and Technology, Changchun, 130022, China
[b] School of Physics and Technology, Key Laboratory of Nuclear Solid State Physics Hubei Province, Wuhan University, Wuhan, 430072, China
[c] Collaborative Innovation Center of Optical Materials and Chemistry, Changchun University of Science and Technology, Changchun, 130022, China
[d] Key Laboratory of Optoelectronic Materials Chemistry and Physics, Fujian Institute of Research on the Structure of Matter, Chinese Academy of Sciences, Fuzhou, 350002, China
[e] School of Materials Science and Engineering, Jilin Jianzhu University, Changchun, 130118, China
[f] Changchun Institute of Optics, Fine Mechanics and Physics, Chinese Academy of Sciences, Changchun, 130033, China

ARTICLE INFO

Keywords:
Tungstate
Up-conversion
Temperature sensing
Phosphor

ABSTRACT

Up-conversion luminescence (UCL) materials have potential applications in many fields. In this work, NaY$(WO_4)_2$(NYW):1 mol%Ho^{3+}/25 mol%Yb^{3+} up-conversion luminescent materials doped with different Gd^{3+} ion concentrations were synthesized by high-temperature solid-state method. X-ray diffraction and infrared absorption spectra show that the incorporation of Gd^{3+} ions increases the lattice parameters and changes the stretching vibration of O–W–O bonds. The properties of the obtained UCL materials were also studied under the excitation of a 980 nm laser. All the samples show strong green and red up-conversion emission peaks centered at 542 nm and 645 nm, which correspond to the Ho^{3+} ion $^5F_4/^5S_2 \rightarrow {}^5I_8$ and $^5F_5 \rightarrow {}^5I_8$ energy levels, respectively. The pumping power coefficient shows that the emission at 542 nm and 645 nm is a two-photon process. The temperature dependence of the red-green emission ratio under 980 nm excitation was studied in the range of 343 K–693 K. According to thermal quenching theory, the fluorescence intensity ratio (FIR) is a function of temperature, and the sensitivity of the obtained phosphor reaches its maximum value at 343 K. These results show that NYW:Ho/Yb/Gd UCL is worthy of further study due to its potential for applications in the fields of up-conversion lasers, bioluminescence labeling, and temperature sensing.

1. Introduction

Up-conversion luminescence (UCL) occurs when the materials emit high-energy light at the excitation of low-energy light. Materials can emit high-frequency short-wavelength light as well, known as anti-Stokes luminescence [1]. Compared with organic fluorophores and semiconductor luminescent materials, UCL materials have good photochemical stability, a sharp emission bandwidth, and large anti-Stokes displacement, which means that discrete emission peaks can be distinguished from infrared excitation [2]. In recent years, these UCL materials have been used in a wide range of applications such as multi-color displays [3], solar energy storage [4], anti-counterfeiting technology [5], biological imaging [6], and temperature sensing [6]. A wide range of inorganic materials with complex structures have been studied, such as borate, molybdate, and tungstate. As an important solid-state luminescent material, rare earth ion-doped tungstate has been widely studied on account of its excellent catalyst performance and wide application prospect in temperature sensor, laser and other fields [7]. Due to its unique structure, tungstate luminescent materials have a strong charge transition absorption spectrum in the low wavenumber

* Corresponding author. School of Materials Science and Engineering, Changchun University of Science and Technology, Changchun 130022, China.
** Corresponding author. School of Materials Science and Engineering, Changchun University of Science and Technology, Changchun 130022, China.
*** Corresponding author. School of Materials Science and Engineering, Changchun University of Science and Technology, Changchun 130022, China.
E-mail addresses: lichun1210@163.com (C. Li), linhaihailin@126.com (H. Lin), zengfm@126.com (F. Zeng).
[1] These authors contributed equally to this work and should be considered co-first authors.

https://doi.org/10.1016/j.physb.2022.414351
Received 5 June 2022; Received in revised form 11 September 2022; Accepted 12 September 2022
Available online 18 September 2022

region and can be mixed with high concentrations of rare earth luminescent ions.

In many lanthanide-doped UCL materials, fluorescence emission is mainly caused by the energy level transition of the unique 4f shell in the electric and magnetic dipole, which leads to sharp emission in a narrow band. Ho^{3+} ion is a commonly used and important activator due to its rich energy level structure and long metastable fluorescence lifetime in the 4f electron layer. However, the 4f–4f transition is forbidden by the electric dipole and Ho^{3+} ions only weakly absorb incident photons, so it is necessary to introduce a sensitizer to realize up-conversion energy transfer in Ho^{3+}-doped UCL materials [8]. When mixed with Yb^{3+} ions, Ho^{3+} ions can produce green and red up-conversion emissions under the excitation of a 980 nm laser. Although the addition of Yb^{3+} ions significantly changes the fluorescence intensity of UCL materials, these materials need to be further developed to meet future application requirements. Therefore, further research on improving the fluorescence intensity of UCL materials by lanthanide doping has become a hot topic. Previously, some scholars enhanced the fluorescence intensity of materials by adding Li^{+} ions [9]. Paudel et al. reduced the radiation-free relaxation process between energy levels by using a cladding method, which increased the intensity of up-conversion luminescence to some extent. Furthermore, it is well known that the luminescence of Ho^{3+} ions is easily affected by the surrounding coordination environment. When the local environment changes, the luminescence color of Ho^{3+} ions undergoes red-green transformation [10]. Therefore, in this study, we realized the regulation of Ho^{3+} ion luminescence by changing the local environment of the crystal structure. We changed the lattice environment of the matrix material by adding Gd^{3+} ions to affect its luminescence intensity. Gd^{3+} ions have a larger radius than Y^{3+} ions, so Gd^{3+} ions are more likely to replace Y^{3+} ions in the lattice and change the symmetry of the lattice field, thus playing a role in regulating the emission of Ho^{3+} ions [11,12].

Temperature detection is a key parameter in scientific research and industrial manufacturing. Temperature-dependent up-conversion emission spectroscopy is often used for non-contact temperature measurements, and fluorescence intensity ratio (FIR) technology is an effective method for accurately measuring temperature. FIR technology is related to the thermal coupling level of energy levels and the sensitivity of FIR sensors is limited to the energy gap range of 200–2000 cm^{-1}, so it is challenging to improve the sensitivity of these temperature sensors. According to the thermal quenching theory, the emission ratio of the red and green up-conversion peaks is a temperature-dependent function in the temperature range of 343 K–693 K. The results showed that with increasing temperature, the absolute sensitivity of $NaY(WO_4)_2$ decreased and the highest absolute sensitivity of 0.002 K^{-1} was obtained at 343 K, indicating that $NaY(WO_4)_2$ has great potential in low-temperature measurement applications.

Therefore, in this study, we prepared $NaY(WO_4)_2$:Ho^{3+}/Yb^{3+} UCL materials doped with Gd^{3+} ions by high-temperature solid-state method. X-ray diffraction (XRD), Fourier infrared absorption spectroscopy (FT-IR), fluorescence spectroscopy, pump power spectroscopy, variable temperature spectroscopy, and a fluorescence decay time test were used to analyze the crystal phase structure, [WO_4] tetrahedron scale transformation, transformation of the fluorescence emission intensity, energy transfer mechanism, and temperature sensing characteristics of the obtained materials in detail.

2. Experimental details

2.1. Preparation

$NaY(WO_4)_2$:1 mol%Ho^{3+}/25 mol%Yb^{3+} doped with different Gd^{3+} ion concentrations was prepared by high-temperature solid-state method. The initial raw materials used in this experiment were sodium carbonate (Na_2CO_3 > 99.99%), tungsten oxide (WO_3 > 99.99%), yttrium oxide (Y_2O_3 > 99.99%), nitrous oxide (Yb_2O_3 > 99.99%), holmium oxide (Ho_2O_3 > 99.99%), and gadolinium oxide (Gd_2O_3 > 99.99%). All of the chemicals were of high purity without further purification. The compositions of the prepared $NaY(WO_4)_2$ materials were 1 mol% Ho^{3+} ions and 25 mol% Yb^{3+} ions, with the remaining 74 mol% Y^{3+} ions in the matrix replaced by 20%, 40%, 60%, 80%, or 100% Gd^{3+} ions. For each material, the raw materials were weighed according to the required stoichiometric ratio. The moles of rare earth ions are shown in Table 1. The weighed powder was then placed in an agate mortar and thoroughly mixed with anhydrous ethanol. After being thoroughly ground, the material was transferred to a corundum crucible, heated for 6 h at 880 °*C*, allowed to cool to room temperature, and then ground again.

2.2. Characterization

The elements in $NaY(WO_4)_2$ were analyzed by X-ray photoelectron spectroscopy (XPS) using an EP13-002 electronic analyzer. The samples were also characterized by X-ray diffraction (XRD; Shimadzu Co., Ltd., Cu $K\alpha_1$ radiation source, target voltage of 40 kV, current of 20 mA, step size of 0.02°, scanning range of 10°–80°). The measurements of Raman spectra were conducted using a LabRam Aramis (type for Horiba Jobin-Yvon, France). The Raman excitation source was employed by an Ar ion laser with 514.5-nm line. The power level was maintained at the 0.5 mW to avoid decomposition of the samples. An FTIR-1500 Fourier-transform infrared (FT-IR) spectroscopy was used to measure the infrared absorption spectra of the powders. An F-7000 fluorescence spectrometer (Hitachi High-Tech, Japan) was used to obtain the fluorescence spectra, and the fluorescence decay curves at 542 nm and 645 nm were determined by spectrophotometer (FLS920, Edinburgh Instruments, UK) under 980 nm excitation. The photoluminescence spectra of the samples with different doping concentrations were also measured by the FLS980 spectrophotometer under 980 nm excitation. The temperatures of the samples were controlled by a temperature-controlled stage between 343 K and 843 K.

3. Results and discussion

3.1. Structures and morphologies

The XRD patterns of sintered $NaY(WO_4)_2$:Ho^{3+}/Yb^{3+} doped with different Gd^{3+} ion concentrations are shown in Fig. 1(a). The diffraction peaks of all the samples are consistent with that of $NaY(WO_4)_2$ (JCPDS#48-0886), and there are no other impurity phases. These sharp and intense peaks indicate that the prepared samples are highly crystalline. $NaY(WO_4)_2$ is a kind of quadrate crystal, and its spatial group is $I4_1/a$. Its lattice constants are a = b = 5.205 Å, c = 11.251 Å, and Z = 2 (the number of molecules in each unit cell). Fig. 2 shows a crystal structure model of $NaY(WO_4)_2$. According to Fig. 1(b), when Gd^{3+} ions are not incorporated into the lattice, the main (112) peak shifts to a larger 2θ angle because the radii of the Ho^{3+} (1.015 Å) and Yb^{3+} (0.985 Å) ions are smaller than that of Y^{3+}(1.019 Å). The crystal structure of the $NaY(WO_4)_2$ cubic phase does not change with Gd^{3+} doping, but the positions of the diffraction peaks shift to lower angles because the ionic radius of Gd^{3+} (1.053 Å) is larger than that of Y^{3+} (1.019 Å) [13,14]. In addition, the effective ion potential is suitable for evaluating the

Table 1
Main compositions of samples and content of doped ions.

Sample	Ho^{3+} ions (mol)	Yb^{3+} ions (mol)	Gd^{3+} ions (mol)
NYW:0Gd^{3+}	0.01	0.25	0
NYW:20%Gd^{3+}	0.01	0.25	0.148
NYW:40%Gd^{3+}	0.01	0.25	0.296
NYW:60%Gd^{3+}	0.01	0.25	0.444
NYW:80%Gd^{3+}	0.01	0.25	0.592
NYW:100%Gd^{3+}	0.01	0.25	0.740

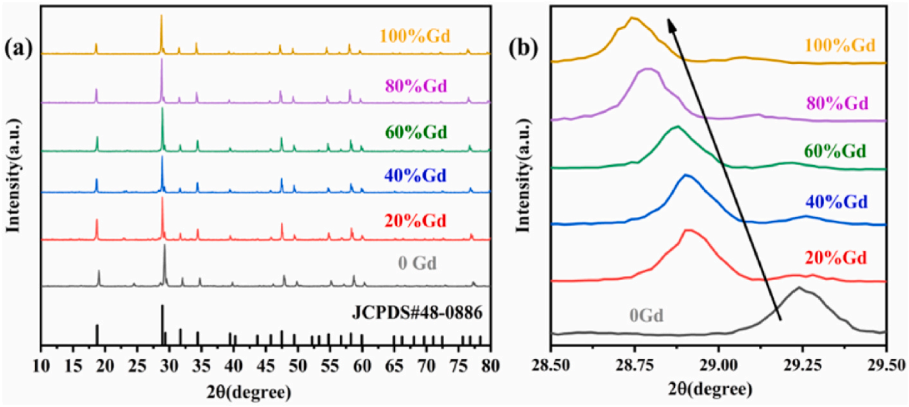

Fig. 1. (a) XRD patterns of NYW:1 mol%Ho^{3+}/25 mol%Yb^{3+} UCL doped with different Gd^{3+} concentrations; (b) Standard data for primary peak and peak (112) of NYW:1 mol%Ho^{3+}/25 mol%Yb^{3+}UCL doped with different Gd^{3+} concentrations.

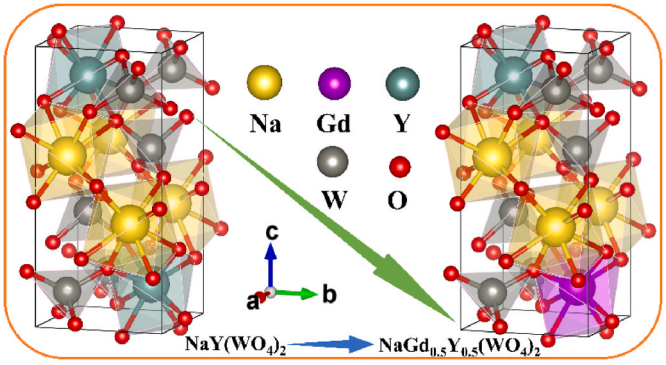

Fig. 2. NYW: Ho/Yb/Gd crystal structure model diagram.

polarization ability of cations, which can be expressed as follows:

$$\varphi_{eff} = Z_{eff}/R \quad (1)$$

Where Z_{eff} is the effective cationic radius and R is the cationic radius of the corresponding ligand. According to Equation (1), when the radius of a doped cation increases, the corresponding polarization intensity will decrease. Therefore, the lattice parameters increase as Y^{3+} ions are replaced in the lattice with Gd^{3+} ions. According to Bragg's law ($2d\sin\theta = n\lambda$), the diffraction angle corresponding to the peak decreases with increasing crystal plane spacing. Therefore, Gd^{3+} replaces Y^{3+} in the $NaY(WO_4)_2$ lattice.

XPS was used to further determine whether Gd^{3+} ions enter the NYW lattice, as shown in Fig. 3(a). All the doped elements exhibit certain binding energy intensities. Fig. 3(b) shows the characteristic $^3d_{5/2}$ and $^3d_{3/2}$ peaks of Gd^{3+}. This is further confirmation that Gd^{3+} ions were successfully incorporated into the $NaY(WO_4)_2$ matrix.

As is well known, $[WO_4]^{2-}$ has a centrosymmetric tetrahedron structure (with W atoms located in the heart of the tetrahedron and O atoms on the vertices). As shown in the FT-IR spectra in Fig. 4, the peak

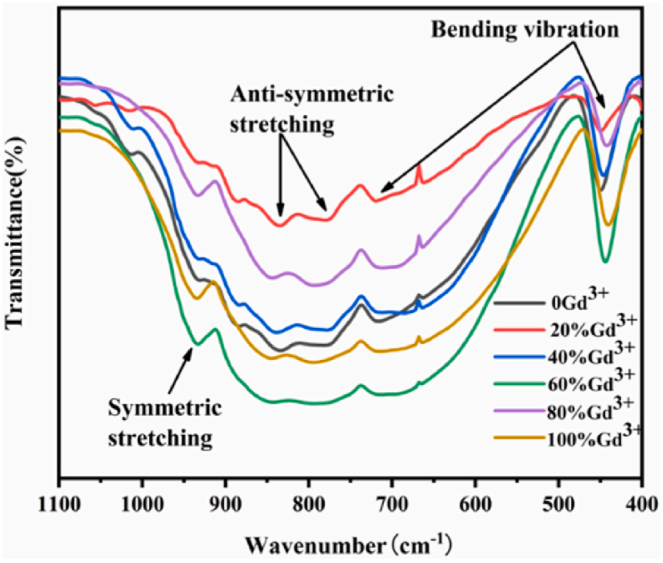

Fig. 4. FT-IR spectra of $[WO_4]$ NYW: Ho^{3+}/Yb^{3+} with different vibrational modes at different Gd^{3+} ion concentrations.

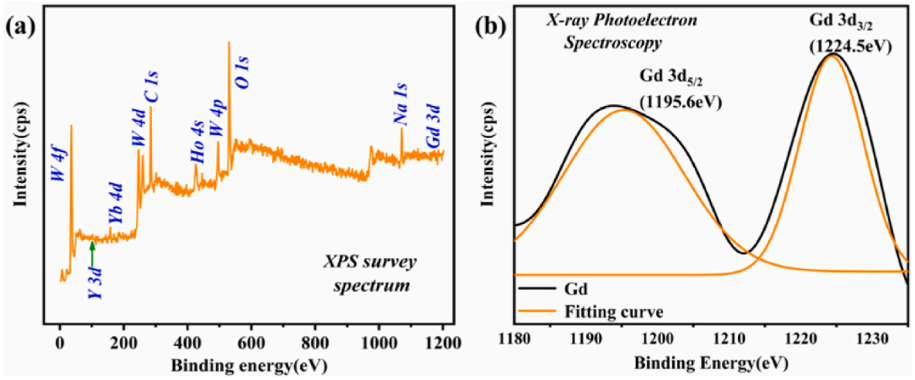

Fig. 3. (a) XPS survey spectrum of Ho^{3+}, Yb^{3+} and Gd^{3+} ions doped NWY samples; (b) XPS spectrum of Gd^{3+}.

at 934 cm^{-1} can be ascribed to the [WO_4] tetrahedron symmetric stretching vibration. The peaks at 777 cm^{-1} and 834 cm^{-1} are attributed to the antisymmetric stretching vibration and bending vibration of O–W–O in the [WO_4] groups, and the peak at 440 cm^{-1} can be attributed to the O–W–O key antisymmetric bending vibration [15]. Fig. 4 shows that the incorporation of Gd^{3+} ions enhances the intensity of vibrations related to the O–W–O bond. This is because the incorporation of Gd^{3+} ions has an impact on Y^{3+} ion sites, which changes the stretching vibration of the O–W–O bond. The bonding strength between atoms is related to their resonance frequency [16]. The addition of Gd^{3+} ions makes the O–W–O bond shorter, so their vibration frequency increases. This result is in good agreement with the XRD analysis, indicating that the addition of Gd^{3+} ions changes the lattice parameters of $NaY(WO_4)_2$. Raman spectroscopy has been used extensively for the analysis and determination of the structure of substances. The Raman spectra of $NaY(WO_4)_2$ powders are shown in Fig. 5. The Raman spectra of $NaY(WO_4)_2$ powders have five main characteristic peaks, 211 cm^{-1}, 332 cm^{-1}, 407 cm^{-1}, 805 cm^{-1} and 916 cm^{-1}, respectively. The stretching vibrational mode of the WO_4^{2-} group leads to the production of a diffraction peak at 916 cm^{-1}. The bending vibration of the WO_4^{2-} group leads to the production of diffraction peaks around 300 cm^{-1}-450 cm^{-1}, the diffraction peak at 805 cm^{-1} is an asymmetric stretching vibration of the WO_4^{2-} group, and the translational vibration mode of the WO_4^{2-} group and the rotational mode of Na^+ and Yb^{3+} lead to the production of diffraction peaks around 190 cm^{-1}-220 cm^{-1}.

3.2. Photoluminescence characteristics

Fig. 6(a) shows PL spectra with two different UCL bands. One is the strong green emission band, with a range of 520–575 nm and a peak of 542 nm. The other is the red emission band, with a wavelength range of 630–675 nm and a peak of 645 nm. The peaks of these two bands correspond to the two radiative transitions of Ho^{3+}, which are $^5F_4/^5S_2 \rightarrow {}^5I_8$ and $^5F_5 \rightarrow {}^5I_8$, respectively. As shown in Fig. 6(b), the green up-conversion luminescence intensity first increases and then decreases with increasing Gd^{3+} concentration. When the doping concentration exceeds the optimal value, Gd^{3+} doping destroys the luminescence cluster structure and causes the luminescence intensity to decrease [17]. The highest luminescence intensity occurs with a Gd^{3+} concentration of 60%. Green emission intensity is increased by 4.57 times higher and red emission intensity by 3.86 times higher compared to the sample without Gd^{3+}, indicating that the addition of Gd^{3+} effectively increases the fluorescence emission intensity of this material [18,19].

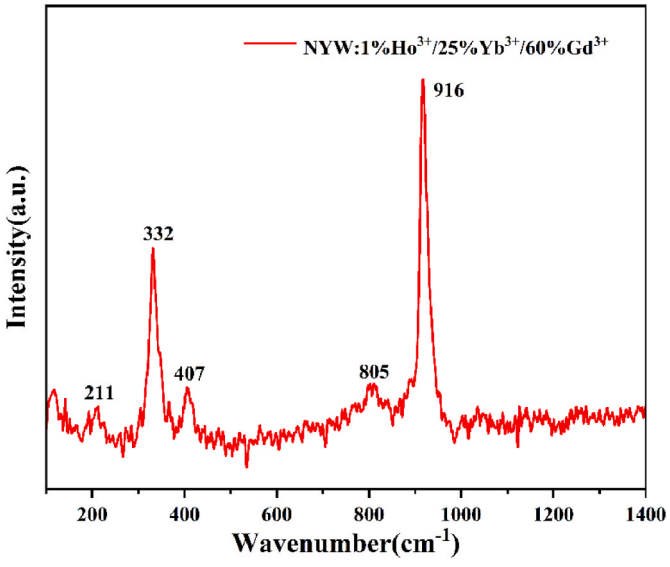

Fig. 5. Raman spectrum of the NYW: Ho/Yb/Gd powder.

In order to further investigate the energy transfer mechanism of Ho^{3+}, we used the relationship between UCL strength and excitation power, which can be expressed as [20]:

$$I \propto P^n \tag{2}$$

Where I is the up-conversion fluorescence emission intensity, P is the power of the pumped laser, and n is the number of 980 nm laser photons needed to generate a UCL photon. As shown in Fig. 7, the peak strength increases as the laser pump power increases. When the pump power reaches 465 mW, the luminescence intensity is 2.76 times of that when the pump power is 285 mW. Fig. 7 shows that the slopes of the emission peaks at 542 nm and 645 nm are 1.965 and 1.971, respectively, which shows that the Ho^{3+} ion photoluminescence processes at $^5F_4/^5S_2$ and $^5I_5$ are both two-photon absorption processes [21,22].

Fig. 8 shows the energy transfer process of Ho^{3+}, Yb^{3+}, and Gd^{3+} under up-conversion excitation. First, a large number of Yb^{3+} ions are absorbed and are excited by the incident photons. Due to the small gap between the Yb^{3+} $^2F_{7/2} \rightarrow {}^2F_{5/2}$ energy levels, these ions usually absorb the lower energy photons at 980 nm (near-infrared) [23,24]. The excited Yb^{3+} ions then transfer energy to Ho^{3+} ions in a back-energy-transfer (BET) process. In this process, Yb^{3+} ions return to the ground state and Ho^{3+} ions are excited. Initially, Ho^{3+} ions are all in their $^5I_8$ ground state energy level. After mutual matching between energy levels, Ho^{3+} ions in the ground state accept the energy transferred from the Yb^{3+} ions and are excited to the $^5I_6$ excited state. Because this excited state is metastable and has a long lifetime, it will not immediately lead to photon emission and a return to the ground state. On account of this, most of the Ho^{3+} ions are still in the $^5I_6$ excited state as Yb^{3+} ions continue to transfer energy to Ho^{3+} ions. Therefore, the Ho^{3+} ions can also be excited by a second energy transfer from $^5I_6$ to $^5F_4/^5S_2$ and $^5I_5$. The particles at the Ho^{3+} $^5F_4/^5S_2$ energy level are distributed through two energy transfers (ET4 and ET5) with Yb^{3+} ions [25]. Then some of the electrons at the $^5F_4/^5S_2$ energy level transition to the ground state of Ho^{3+}, while other electrons transition to the $^5I_7$ energy level of Ho^{3+} and emit near-infrared light. In addition, some electrons are transferred to the $^2F_{5/2}$ energy level of Yb^{3+} by the BET process [$^5F_4/^5S_2(Ho)+{}^2F_{7/2}(Yb) \rightarrow {}^5I_6(Ho)+{}^2F_{5/2}(Yb)$]. The population of the $^5F_5$ level is realized through two processes: the radiation-free relaxation of the Ho^{3+} $^5F_4/^5S_2$ level and the two energy transfer processes of Yb^{3+}. The ET4 process is the result of the combined action of the radiation-free relaxation of $^5I_6 \rightarrow {}^5I_7$, the CR of $^5F_4/^5S_2(Ho)+{}^5I_8(Ho) \rightarrow {}^5I_4(Ho)+{}^5I_7(Ho)$, and the radiation process of $^5F_4/^5S_2 \rightarrow {}^5I_7$. Because the two $^5F_4/^5S_2$ and $^5I_5$ energy levels have a short lifetime, they lead to an energy level transition to $^5I_8$ and emit green light at around 550 nm and red light at around 650 nm, respectively. This luminescence process is referred to two-photon process because it requires the participation of two photons [26,27].

Figs. 9(a) and 10(a) show the Ho^{3+} logarithmic decay curves of $^5F_4/^5S_2$ at 542 nm and $^5F_5$ at 645 nm with different Gd^{3+} doping concentrations. The fluorescence decay curves of the different energy levels of Ho^{3+} ions in the $NaY(WO_4)_2$ lattice are well-fitted by the following double exponentials [28]:

$$I(t) = I_0 + A_1 \exp(-t/\tau_1) + A_2 \exp(-t/\tau_2) \tag{15}$$

Where I_0 represents the luminescence intensity measured at the initial time and I(t) represents the luminescence intensity measured at time t. A_1 and A_2 are constants, t denotes time, and τ_1 and τ_2 denote the fluorescence decay time in the exponential composition. According to these parameters, the mean fluorescence decay time can be calculated with the following equation [28]:

$$\tau = \left(A_1\tau_1^2 + A_2\tau_2^2\right) / \left(A_1\tau_1 + A_2\tau_2\right) \tag{16}$$

Table 2 shows the average fluorescence decay time of Ho^{3+} emission at 542 nm and 645 nm under 980 nm excitation. It can be seen that the decay times of $^5F_4/^5S_2$ and $^5F_5$ energy levels of Ho^{3+} increase with the

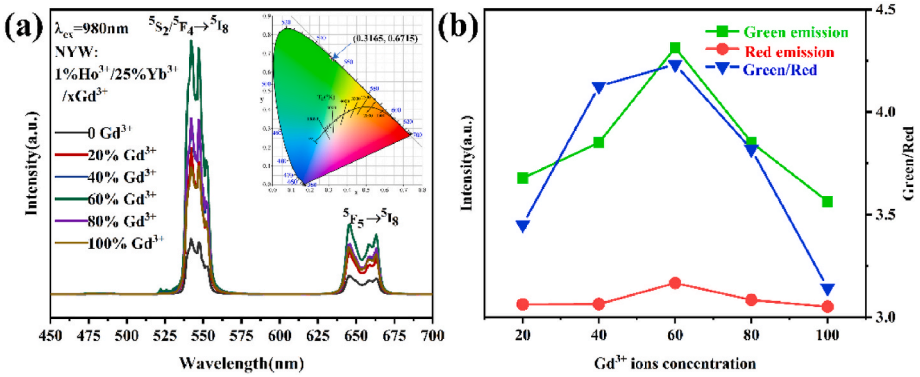

Fig. 6. (a)Up-conversion emission spectra of NYW: Ho^{3+}/Yb^{3+} doped with different Gd^{3+} ion concentrations at 980 nm pump source; (b) The function of the concentration of Gd^{3+} with green and red emission intensity and red-green peak ratio. (For interpretation of the references to color in this figure legend, the reader is referred to the Web version of this article.)

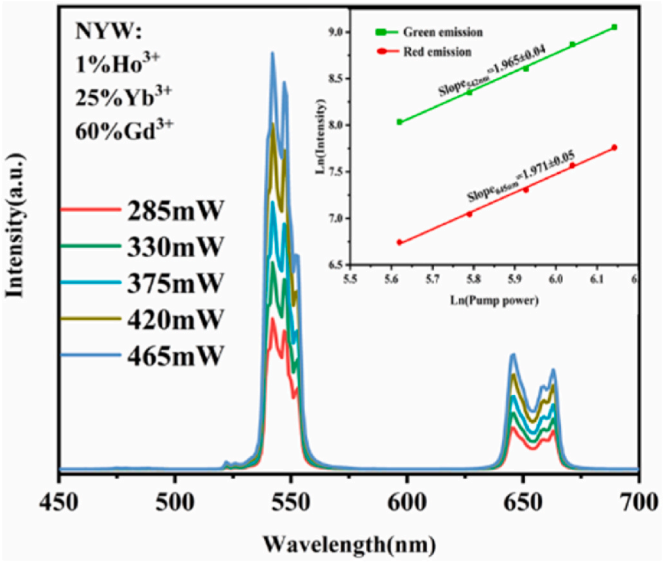

Fig. 7. NYW:Ho^{3+}/Yb^{3+} power spectra doped with 60%Gd^{3+} ions; The logarithmic relationship between up-conversion luminescence intensity and pump power density.

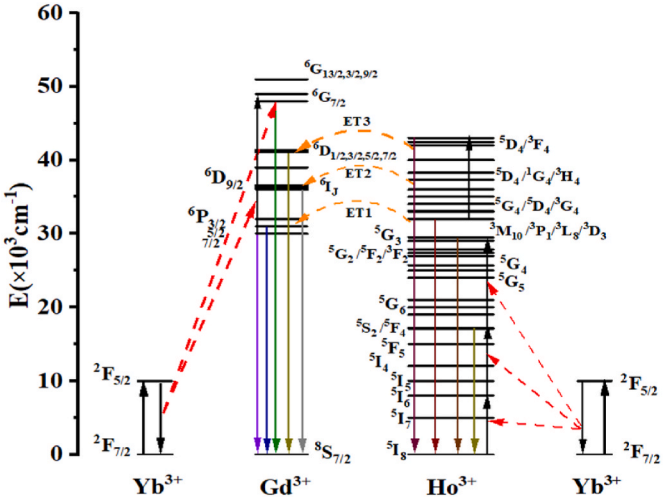

Fig. 8. The UCL energy transfer process of Yb^{3+}, Ho^{3+} and Gd^{3+}.

incorporation of Gd^{3+}. This phenomenon is due to that the incorporation of Gd^{3+} affected the spontaneous radiative transition and non-radiative transition processes [29], lengthening the decay time of the luminescent energy levels. The energy transfer efficiency can be expressed as [30]:

$$\eta = 1 - \tau_0/\tau_s \quad (17)$$

Where η is the energy transfer efficiency, τ_0 is the energy level lifetime in the absence of Gd^{3+}, and τ_s is the energy level lifetime with Gd^{3+}. As shown in Figs. 9(b) and 10(b), the energy transfer efficiency increases with increasing Gd^{3+} concentration and Gd^{3+} enhances the energy transfer efficiency by 45.27%.

In order to better explain the up-conversion luminescence mechanism of Gd^{3+}-doped $NaY(WO_4)_2$:Ho^{3+}/Yb^{3+}, the band structures and densities of the state of $NaY(WO_4)_2$ and $NaYGd(WO_4)_2$ were calculated. All calculations were based on spin polarization density functional theory (DFT) and calculated by VASP software. The Perdew-Burke-Ernzerhof (PBE) generalized gradient approximation (GGA) was used for exchange and correlation correction. The pseudopotential wave was set to projection enhanced wave (PAW) to describe the core electrons. The valence/exonuclear electrons for each atom in self-consistent field calculations are expressed in brackets for the following atoms: W ([Xe] $4f^{14}5d^46s^2$), Y ([Kr]$4d^15s^2$), Gd ([Xe]$4f^75d^16s^2$), Na (3 S^1), and O ($2s^22p^4$). The U_{eff} values of W, Y, and Gd were set to 4.0, 2.0, and 6.0 eV for the Hubbard correction. The plane wave cutoff energy was set at 450 eV, K was 5 × 5 × 3, and the convergence standards of energy and force were set to 10^{-5} eV and 0.01 eVa^{-1}, respectively.

Fig. 11 shows the calculated band structure diagram. The band gap of $NaY(WO_4)_2$ is 2.64 eV (Fig. 11(a)), and when doped with Gd^{3+}, the calculated band gap is 2.66 eV (Fig. 11(b)). There is almost no difference in the band gap between the two samples. These results show that Gd^{3+} ion doping does not create impurity levels in the band gap and does not reduce the band gap width to improve the luminescence performance of $NaY(WO_4)_2$:Ho^{3+}/Yb^{3+}. The densities of state can more clearly explain this point. As shown in Fig. 12, Gd^{3+} ion doping causes the change at 4.7 eV. This is because Gd^{3+} and Y^{3+} have similar outer electron structures except for the addition of *f*-layer electrons. These *f*-orbital electrons are not distributed near the Fermi energy level (0 eV), so they mostly do not participate in the electron transition. However, by comparing the band change between the lower part of the conduction band and the top part of the valence band, it can be inferred that the improvement in optical performance by Gd^{3+} ion doping is realized by these changes (Fig. 11 (c)). Table 3 shows the effective mass of carriers in the G-A, G-B, and G-Y directions. The results show that after Gd^{3+} ion doping, band structure changes in the G-A and G-Y directions lead to a decrease in the effective mass of carriers (electrons and holes). When excited at 980 nm, the carrier mobility is effectively improved. Furthermore, the probability of carrier and phonon energy scattering during the energy transfer is

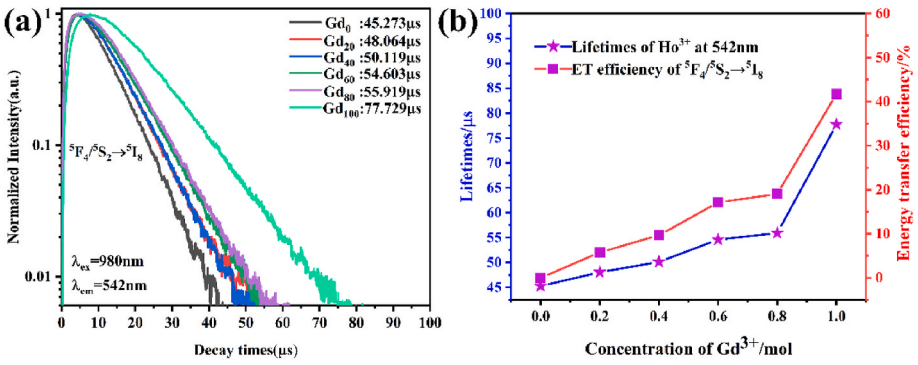

Fig. 9. (a) Fluorescence decay time of Ho^{3+} $^5F_4/^5S_2$ energy level doped with different Gd^{3+} concentration; (b) Effects of Gd^{3+} ions on the lifetime and energy transfer efficiency of $^5F_4/^5S_2$ level.

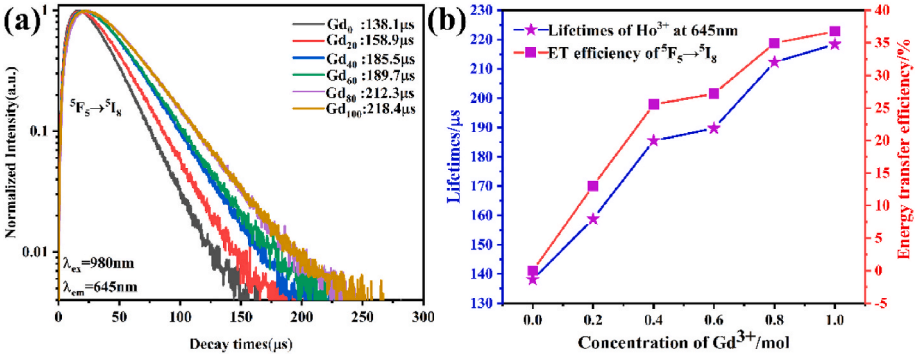

Fig. 10. (a). Fluorescence decay time of Ho^{3+} $^5F_5$ energy level doped with different Gd^{3+} concentration; (b) Effects of Gd^{3+} ions on the lifetime and energy transfer efficiency of $^5F_5$ level.

Table 2
The enhancement and decay time of green and red emission peaks after addition of Gd^{3+} ions.

Sample (λ_{ex} = 980 nm)	τ (λ_{em} = 542 nm)	τ (λ_{em} = 645 nm)
NYW: Gd_0	45.273 ± 0.083 μs	138.1 ± 0.287 μs
NYW: Gd_{20}	48.046 ± 0.077 μs	158.9 ± 0.049 μs
NYW: Gd_{40}	50.119 ± 0.085 μs	185.5 ± 0.399 μs
NYW: Gd_{60}	54.603 ± 0.085 μs	189.7 ± 0.394 μs
NYW: Gd_{80}	55.919 ± 0.015 μs	212.3 ± 0.457 μs
NYW: Gd_{100}	77.729 ± 0.016 μs	218.4 ± 0.505 μs

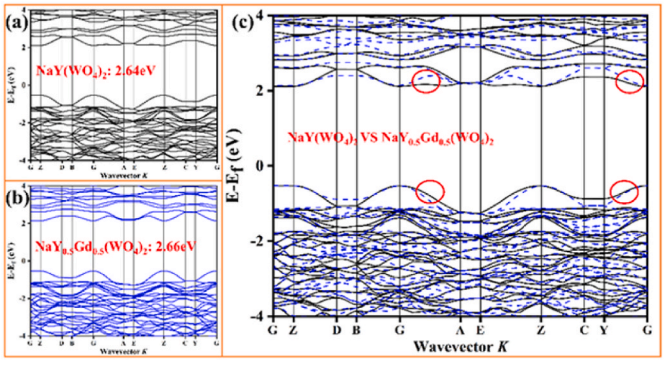

Fig. 11. (a) The band gap of $NaY(WO_4)_2$; (b) The band gap of $Na_{0.5}Gd_{0.5}Y(WO_4)_2$; (c) Comparison of band structure before and after doping.

reduced and the luminescence performance of the material is improved. This is the first time this phenomenon has been reported, and these results provide a new theoretical basis and insight for Gd^{3+} ion doping to improve the luminescence performance of UCL materials.

3.3. Temperature sensing characteristics

The laser source was a 980 nm semiconductor laser and the emitted spectrum was received by a spectrometer. The phosphor with a thickness of 0.5 mm is fixed in a home-made tubular heating furnace, through which the powder is heated. This system is fixed in a sealed chamber with a quartz window to prevent heat loss during temperature transfer [31]. Upconversion spectra were recorded at 50 K intervals over the temperature range 343 K–843 K. To ensure the accuracy of the temperature measurement, the spectrum was collected after the temperature had risen to the desired temperature by staying and observing until the spectrum had stabilised. An important factor affecting the up-conversion efficiency of rare earth ions is the multiphonon non-radiative relaxation rate (W_{NR}) [32]:

$$W_{NR} \propto [1 - \exp(-h\nu/k_bT)]^{-P} \quad (18)$$

Where hυ is the phonon energy around the medium, h is Planck's constant, ν is the vibration frequency, k_b is the Boltzmann constant, T is the absolute temperature, and P is the phonon number needed to replenish the upper and lower energy levels. Equation (18) shows that a medium with low phonon energy reduces the non-radiative relaxation rate of multiple phonons and thus increases luminescence. The multi-photon relaxation process is competitive with the radiation process in this temperature-dependent study when the energy gap of the equivalent level is equal to 3–4 times the phonon energy.

The temperature sensing properties of the $NaY(WO_4)_2$:1%Ho^{3+}/25% Yb^{3+}/60%Gd^{3+} phosphor were studied because the highest up-conversion emission peaks were obtained with this sample. Fig. 13 shows that the up-conversion emission intensities at 343 K–843 K

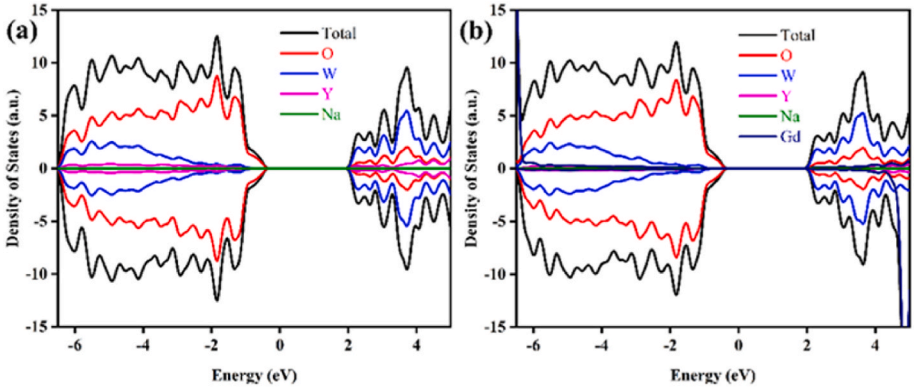

Fig. 12. (a) The DOS of $NaY(WO_4)_2$; (b) The DOS of $Na_{0.5}Gd_{0.5}Y(WO_4)_2$.

Table 3
The effective mass of carrier.

Sample	G-A		G-B		G-Y	
	holes	Electrons	holes	Electrons	holes	Electrons
$NaY(WO_4)_2$	−2.73	3.60	−1.87	1.67	−1.74	2.11
Gd:NaY $(WO_4)_2$	−1.23	1.23	−1.58	2.01	−1.74	1.63

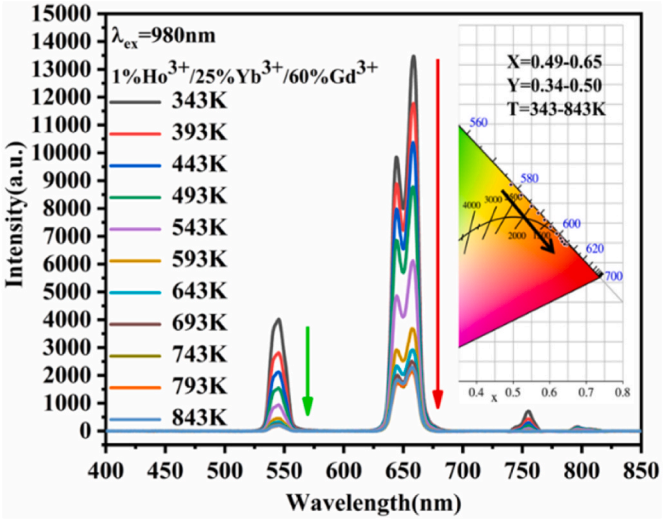

Fig. 13. Up-conversion emission spectra of NYW: $Ho^{3+}/Yb^{3+}/60\%Gd^{3+}$ at the temperature range from 343 to 843 K, inset shows CIE chromaticity diagram with NYW: $Ho^{3+}/Yb^{3+}/60\%Gd^{3+}$ at the temperature range from 343 to 693 K.

gradually decrease with increasing temperature, while the peak positions do not significantly shift. This phenomenon is conducive to thermal agitation. As the non-radiative relaxation of electrons between rare earth ions increases, the intensity of the emission peak decreases with increasing temperature. The intensity of the red up-conversion emission peak rapidly decreases, while the intensity of the green up-conversion emission peak only slightly decreases, resulting in a significant decrease in the FIR (I_{658}/I_{545}). Furthermore, as shown by Fig. 13, the light released by the sample between 343 K and 843 K gradually approaches the red light in the CIE chromaticity diagram and the coordinate value increases with increasing temperature. In addition, the FIR from the green up-conversion emission of $^5F_4/^5S_2$–$^5I_8$ and the red up-conversion emission of $^5F_5$–$^5I_8$ can be expressed as [33]:

$$FIR = I_{658} / I_{545} = A\exp[-\triangle E/(k_b T)] + B \quad (19)$$

Where I_{658} is the emission intensity of $^5F_5$–$^5I_8$, I_{545} is the emission intensity of $^5F_4/^5S_2$–$^5I_8$, A and B are nonlinear fitting constants, ΔE is the energy gap between $^5F_4/^5S_2$–$^5I_8$ and $^5F_5$–$^5I_8$, k_b is the Boltzmann constant, and T is the absolute temperature. Fig. 14 shows the up-conversion emission intensities and their ratios at 545 nm and 658 nm in the temperature range of 343 K–693 K. As the influence of temperature on the phonon energy of the matrix increases, the non-radiative relaxation rate between electrons also increases. Therefore, the FIR decreases from 3.592 to 0.857 when the temperature increases from 343 K to 693 K. By fitting the experimental data with Equation (19), the coefficients A, B, ΔE/k, and R^2 in Fig. 14 are 3.286, 2.553, 235.29, and 0.998, respectively. In addition, material sensitivity is very important for temperature sensing applications, defined as the rate at which the FIR changes with temperature. Sensor sensitivity can be defined as:

$$Sr = d(FIR) / dT = FIR[\triangle E / (k_b T^2)] \quad (20)$$

Fig. 15 shows the sensitivity of $NaY(WO_4)_2$:1%Ho^{3+}/25%Yb^{3+}/60%Gd^{3+} to temperature. The absolute sensitivity of this material gradually decreases with increasing temperature. The maximum sensitivity of this sample is 0.002 at 343 K and the minimum sensitivity is 4.9×10^{-4} at 693 K. These results indicate that $NaY(WO_4)_2$ phosphor doped with lanthanide ions has good temperature sensing properties and is a potential temperature sensing material.

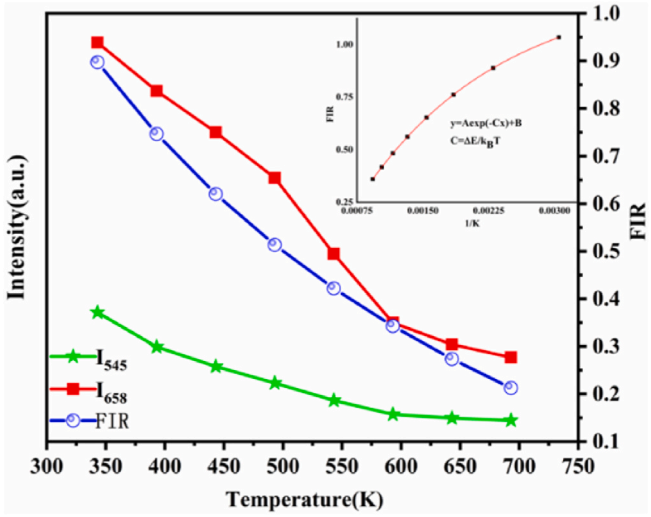

Fig. 14. Intensity ratio of 545 nm–658 nm with the temperature range from 343 to 693 K, inset shows the fitting function of FIR-T.

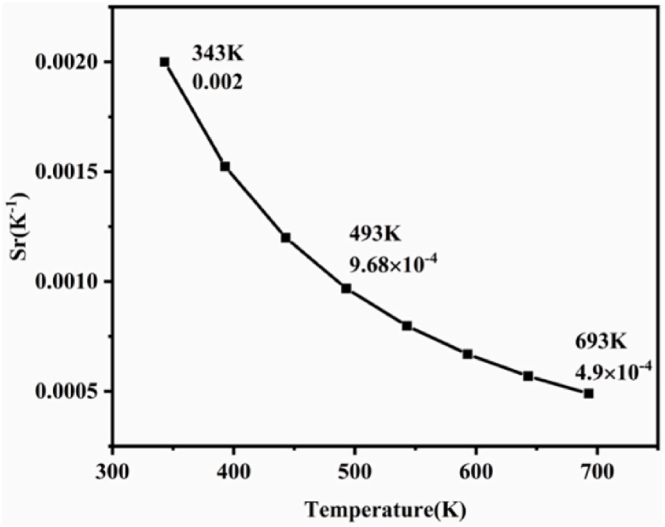

Fig. 15. Sensing sensitivity of NYW: $Ho^{3+}/Yb^{3+}/60\%Gd^{3+}$ as a function of temperature.

4. Conclusion

In summary, $NaY(WO_4)_2$:1 mol%Ho^{3+}/25 mol%Yb^{3+} UCL materials doped with different Gd^{3+} ion concentrations were prepared by high-temperature solid-state method. XRD analysis showed that because the ionic radius of Gd^{3+} is larger than that of Y^{3+}, the diffraction peak shifts to a smaller angle with the addition of Gd^{3+} ions, the crystal plane spacing becomes larger, and the main lattice therefore expands. Furthermore, the incorporation of Gd^{3+} ions modifies Y^{3+} ion sites, affecting the stretching vibration of O–W–O bonds, increasing the vibration frequency, and increasing the total energy of lattice vibration. The Ho^{3+} luminescent energy level absorbs phonon energy, improving UCL performance. Under the excitation of a 980 nm laser, all the samples showed two sharp emission peaks located at 542 nm and 645 nm, respectively corresponding to the $^5S_2/^5F_4 \rightarrow {}^5I_8$ and $^5F_5 \rightarrow {}^5I_8$ energy transfers of Ho^{3+}. Furthermore, with the addition of Gd^{3+} ions, the luminescence intensity of the green and red emission peaks increased by 4.57 and 3.86 times, respectively. When Gd^{3+} doping concentrations higher than 60%, the luminescence intensity declined due to excessive destruction of the fluorescence clusters by Gd^{3+}. The measured power show that the transitions of the Ho^{3+} luminescent energy level are two-photon processes. The steady-state rate equation was used to theoretically show that the enhanced green and red conversion emission intensities were caused by the expansion of the main lattice and the increase of the $^5S_2/^5F_4$ and $^5F_5$ energy level lifetimes. The relationship between the temperature-dependent up-conversion emission spectrum and the luminescence intensity ratio confirmed the potential for using $NaY(WO_4)_2$ phosphors in temperature sensors, with a maximum sensitivity of 0.002 K^{-1}. Therefore, these materials show great promise as low-temperature warning indicators.

CRediT authors statement

Hongbin Li: Conceptualization, Data curation, Formal analysis, Writing - original draft. **Jiaqi Zhao**: Data curation, Software, Formal analysis, Writing - editing. **Wenjing Yang**: Formal analysis, Writing - review. **Tianqing Zhang**: Formal analysis, Methodology. **Mengjia Chen**: Investigation, Methodology. **Weiling Yang**: Investigation, Methodology. **Hongyuan Sha**: Investigation, Methodology. **Chun Li**: Investigation, Methodology. **Huisheng Liu, Yongtao Li, Zhiming Shi, Shanli Zhang**: Conceptualization, Supervision, Funding acquisition, Resources, Supervision. **Fanming Zeng**: Conceptualization, Supervision, Funding acquisition, Resources, Supervision. **Zhongmin Su**: Conceptualization, Supervision, Funding acquisition, Resources, Supervision.

Declaration of competing interest

The authors declare that they have no known competing financial interests or personal relationships that could have appeared to influence the work reported in this paper.

Data availability

Data will be made available on request.

Acknowledgements

This work was supported by Government Funded Projects (627010104), International Science Technology Cooperation Project of Jilin Province Science, Technology Department (20200801038GH) and Key Laboratory for Comprehensive Energy Saving of Cold Regions Architecture of Ministry of Education, Jilin Jianzhu University (JLZHKF022021001).

References

[1] R.F. Goncalves, L.S. Cavalcante, I.C. Nogueira, E. Longo, M.J. Godinho, J. C. Sczancoski, R. Mastelaro, I.M. Pinatti, I.L.V. Rosa, A.P.A. Marques, Rietveld refinement, cluster modelling, growth mechanism and photoluminescence properties of $CaWO_4:Eu^{3+}$ microcrystals, CrystEngComm 17 (7) (2015) 1654–1666, https://doi.org/10.1039/C4CE02279C.

[2] Y.B. Zhai, X.Q. Yang, F. Wang, Z.X. Li, G.L. Ding, Z.F. Qiu, Y. Wang, Y. Zhou, S. T. Han, Infrared-Sensitive memory based on direct-grown MoS_2-upconversion-nanoparticle heterostructure, Adv. Mater. 30 (49) (2018), 1803563, https://doi.org/10.1002/adma.201803563.

[3] L.L. Li, L. Liu, W.W. Zi, H. Yu, S.C. Gan, G.J. Ji, H.F. Zou, X.C. Xu, Synthesis and luminescent properties of high brightness $MLa(WO_4)_2$: Eu^{3+} (M=Li, Na, K) and $NaRE(WO_4)_2$: Eu^{3+}(RE=Gd, Y, Lu) red phosphors, J. Lumin. 143 (2013) 14–20, https://doi.org/10.1016/j.jlumin.2013.04.031.

[4] P.K. Tawalare, P.D. Belsare, S.V. Moharil, Semiconductor host for designing phosphors for modification of solar spectrum, Opt. Mater. 100 (2020), 109668, https://doi.org/10.1016/j.optmat.2020.109668.

[5] H.H. Tan, S.W. Xie, J.X. Xu, N. Li, C.F. Zhang, L.J. Xu, J. Zheng, Branched $NaYF_4$: Yb, Er up-conversion phosphors with luminescent properties for anti-counterfeiting application, Sci. Adv. Mater. 9 (12) (2017) 2223–2233, https://doi.org/10.1166/sam.2017.3252.

[6] G. Ajithkumar, B. Yoo, D.E. Goral, P.J. Hornsby, A.L. Lin, U. Ladiwala, V.P. Dravid, D.K. Sardar, Multimodal bioimaging using a rare earth doped Gd_2O_2S: Yb/Er phosphor with upconversion luminescence and magnetic resonance properties, J. Mater. Chem. B 1 (11) (2013) 1561–1572, https://doi.org/10.1039/C3TB00551H.

[7] P. Du, L. Luo, J.S. Yu, Upconversion emission, cathodoluminescence and temperature sensing behaviors of Yb^{3+} ions sensitized $NaY(WO_4)_2$: Er^{3+} phosphors, Ceram. Int. 42 (5) (2016) 5635–5641, https://doi.org/10.1016/j.ceramint.2015.12.083.

[8] H. Zheng, B.J. Chen, H.Q. Yu, J.S. Zhang, J.S. Sun, X.P. Li, M. Sun, B.N. Tian, S. B. Fu, H. Zhong, B. Dong, R.N. Hua, H.P. Xia, Microwave-assisted hydrothermal synthesis and temperature sensing application of Er^{3+}/Yb^{3+} doped $NaY(WO_4)_2$ microstructures, J. Colloid Interface Sci. 420 (2014) 27–34, https://doi.org/10.1016/j.jcis.2013.12.059.

[9] J.H. Chung, J.H. Ryu, S.Y. Lee, B.G. Choi, K.B. Shim, Yellow lighting upconversion from Yb^{3+}/Ho^{3+} co-doped CaMoO4, Mater. Res. Bull. 47 (8) (2012) 1991–1995, https://doi.org/10.1016/j.materresbull.2012.04.014.

[10] X.C. Yu, Y.B. Qin, M.L. Gao, L. Duan, Z.Q. Jiang, L. Gou, P. Zhao, Z. Li, Hydrothermal synthesis and upconversion luminescence of $NaGd(WO_4)_2$ co-doped with Ho^{3+} and Yb^{3+}, J. Lumin. 153 (2014) 1–4, https://doi.org/10.1016/j.jlumin.2014.02.033.

[11] H. Yao, H. Shen, Q. Tang, C. Feng, Y.F. Li, Effect of Li co-doping with Er on up-conversion luminescence property and its temperature dependence of $NaY(WO_4)_2$, J. Phys. Chem. Solid. 126 (2019) 189–195, https://doi.org/10.1016/j.jpcs.2018.11.009.

[12] H.P. Paudel, L. Zhong, K. Bayat, M.F. Baroughi, S. Smith, C. Lin, C.Y. Jiang, M. T. Berry, P.S. May, Enhancement of near-infrared-to-visible upconversion luminescence using engineered plasmonic gold surfaces, J. Phys. Chem. C 115 (39) (2011) 19028–19036, https://doi.org/10.1021/jp206053f.

[13] D.T. Klier, M.U. Kumke, Upconversion luminescence properties of NaYF4: Yb:Er nanoparticles codoped with Gd^{3+}, J. Phys. Chem. C 119 (6) (2015) 3363–3373, https://doi.org/10.1021/jp5103548, 7.

[14] X.F. Shi, J.G. Li, X.J. Wang, Q. Zhu, B.N. Kim, X.D. Sun, Facile hydrothermal crystallization of $NaLn(WO_4)_2$(Ln= La-Lu,and Y), phase/morphology evolution,

and photoluminescence, Sci. Technol. Adv. Mater. 18 (1) (2017) 741–754, https://doi.org/10.1080/14686996.2017.1379342.
[15] T. Li, Y.M. Li, R. Luo, Z.L. Ning, Y. Zhao, M.J. Liu, X. Lai, C. Zhong, C. Wang, J. Q. Zhang, J. Bi, D.J. Gao, Novel Ba $(Gd_{1-x}Y_x)_{0.78}F_5$:20mol%Yb^{3+},2mol%Tm^{3+} ($0 \leq x \leq 1.0$) solid solution nanocrystals: a facile hydrothermal controlled synthesis, enhanced upconversion luminescent and paramagnetic properties, J. Alloys Compd. 740 (2018) 1204–1214, https://doi.org/10.1016/j.jallcom.2018.01.040.
[16] M.Z. Yang, Y. Sui, S. Lü, M.J. Wang, X.J. Wang, M.H. Wu, Y. Wang, T.Q. Lu, W. F. Liu, Effect of Bi^{3+} doping on the quenching concentration of $^2H_{11/2}/^4S_{3/2}$ level of Er^{3+}, J. Alloys Compd. 509 (34) (2011) 8590–8594, https://doi.org/10.1016/j.jallcom.2011.06.037.
[17] I.M. Pinatti, I.C. Nogueira, W.S. Pereira, P.F.S. Pereira, R.F. Gonçalves, J.A. Varela, E. Longo, Rosa ILV Structural and photoluminescence properties of Eu^{3+} doped α-Ag_2WO_4 synthesized by the green coprecipitation methodology, Dalton Trans. 44 (40) (2015) 17673–17685, https://doi.org/10.1039/C5DT01997D.
[18] C.Y. Zhang, X.Y. Wang, C. Li, H. Lin, F.M. Zeng, Z.M. Su, Effect of Li ions on structure and spectroscopic properties of $NaY(WO_4)_2$:Yb/Ho phosphor, Ceram. Int. 46 (15) (2020) 24248–24256, https://doi.org/10.1016/j.ceramint.2020.06.205.
[19] E. Laredo, N. Suarez, A. Bello, Clustering of Y^{3+} in BaF_2 using Gd^{3+} as paramagnetic probes, Solid State Ionics 37 (2–3) (1990) 103–113, https://doi.org/10.1016/0167-2738(90)90233-H.
[20] F. Pellé, N. Gardant, F. Auzel, Effect of excited-state population density on nonradiative multiphonon relaxation rates of rare-earth ions, JOSA B 15 (2) (1998) 667–679, https://doi.org/10.1364/JOSAB.15.000667.
[21] W. Xu, X.Y. Gao, L.J. Zheng, Z.G. Zhang, W.W. Cao, Short-wavelength upconversion emissions in Ho^{3+}/Yb^{3+} codoped glass ceramic and the optical thermometry behavior, Opt Express 20 (16) (2012) 18127–18137, https://doi.org/10.1364/OE.20.018127.
[22] Y. Yang, H. Feng, X.G. Zhang, Microwave heating synthesis and luminescence of $NaY(WO_4)_2$:(Ho^{3+},Yb^{3+}) phosphors, J. Mater. Sci. Mater. Electron. 26 (1) (2015) 229–233, https://doi.org/10.1007/s10854-014-2388-y.
[23] F. Lahoz, I.R. Martin, J.M. Calvilla-Quintero, Ultraviolet and white photon avalanche upconversion in Ho^{3+}-doped nanophase glass ceramics, Appl. Phys. Lett. 86 (5) (2005), 051106, https://doi.org/10.1063/1.1861975.
[24] X.Y. Wang, C.Y. Zhang, D. Hu, W.B. Li, H. Lin, F.M. Zeng, C. Li, Z.M. Su, Influence of Yb ions concentration on Ho: BaY_2F_8 crystals emission in the range of 1–3μm, Opt. Mater. 109 (2020), 110141, https://doi.org/10.1016/j.optmat.2020.110141.
[25] K.M. Deng, T. Gong, L.X. Hu, X.T. Wei, Y.H. Chen, M. Yin, Efficient near-infrared quantum cutting in $NaYF_4$:Ho^{3+}, Yb^{3+} for solar photovoltaics, Opt Express 19 (3) (2011) 1749–1754, https://doi.org/10.1364/OE.19.001749.
[26] G.Y. Chen, G. Somesfalean, Y. Liu, Z.G. Zhang, Q. Sun, F.P. Wang, Upconversion mechanism for two-color emission in rare-earth-ion-doped ZrO_2 nanocrystals, Phys. Rev. B 75 (19) (2007), 195204, https://doi.org/10.1103/PhysRevB.75.195204.
[27] Y.Q. Hu, Q.Y. Shao, X.Y. Deng, J.Q. Jiang, Thermal-responsive multicolor emission of single $NaGdF_4$: Yb/Ce/Ho up-conversion nanocrystals for anticounterfeiting application, Nanophotonics 9 (9) (2020), https://doi.org/10.1515/nanoph-2020-0136.
[28] Z.X. Shi, J. Wang, X. Guan, Upconversion multicolor tuning of $NaY(WO_4)_2$: Tb^{3+} with Eu^{3+} doping, J. Rare Earths 36 (9) (2018) 911–916, https://doi.org/10.1016/j.jre.2018.01.021.
[29] W. Zhang, R.D. Zhang, S.D. Yang, R. Wang, L.Y. Na, R.N. Hua, Synthesis and photoluminescent features of Eu^{3+} doped $NaGd(WO_4)_2$ nanophosphors, Mater. Res. Bull. 122 (2020), 110689, https://doi.org/10.1016/j.materresbull.2019.110689.
[30] Z. Shi, J. Wang, X. Guan, Upconversion multicolor tuning of $NaY(WO_4)_2$: Tb^{3+} with Eu^{3+} doping, J. Rare Earths 36 (9) (2018) 911–916, https://doi.org/10.1016/j.jre.2018.01.021.
[31] N. Rakov, Tm^{3+}, Yb^{3+}: Y_2SiO_5 up-conversion phosphors: exploration of temperature sensing performance by monitoring the luminescence emission, Phys. B Condens. Matter 628 (2022), 413572, https://doi.org/10.1016/j.physb.2021.413572.
[32] Z.S. Zou, T. Wu, H. Lu, Y.Y. Tu, S.L. Zhao, S.C. Xie, F. Han, S.Q. Xu, Structure, luminescence and temperature sensing in rare earth doped glass ceramics containing $NaY(WO_4)_2$ nanocrystals, RSC Adv. 8 (14) (2018) 7679–7686, https://doi.org/10.1039/C8RA00190A.
[33] H. Sha, Z. He, C. Li, et al., Lanthanide-doped Sc2O3 for highly sensitive temperature sensor, Opt. Mater. 93 (2019) 39–43, https://doi.org/10.1016/j.optmat.2019.04.067.